

Fig. 1 H&E staining of skin tissue showing microscopic features of (a) nodular BCC and (b) SCC.

Raman setup

Ex vivo Raman measurements were acquired from the lesion areas of 22 skin tissue biopsies using the conventional mode (back-scattering) and the SORS mode of a custom-built Raman system, previously optimized on skin tissue phantoms with

geometry and optical properties similar to skin (Fig. 2).²⁴ A 785 nm laser (Mini-Benchtop Stabilized Laser, Coherent, Santa Clara, CA, USA) was focused on the sample through a multi-mode fiber (M43L01, Thorlabs), which was in turn coupled to a standard probe with a 4 cm long and 11 mm working distance probe tip (Wasatch Photonics, Morrisville, NC, USA). A

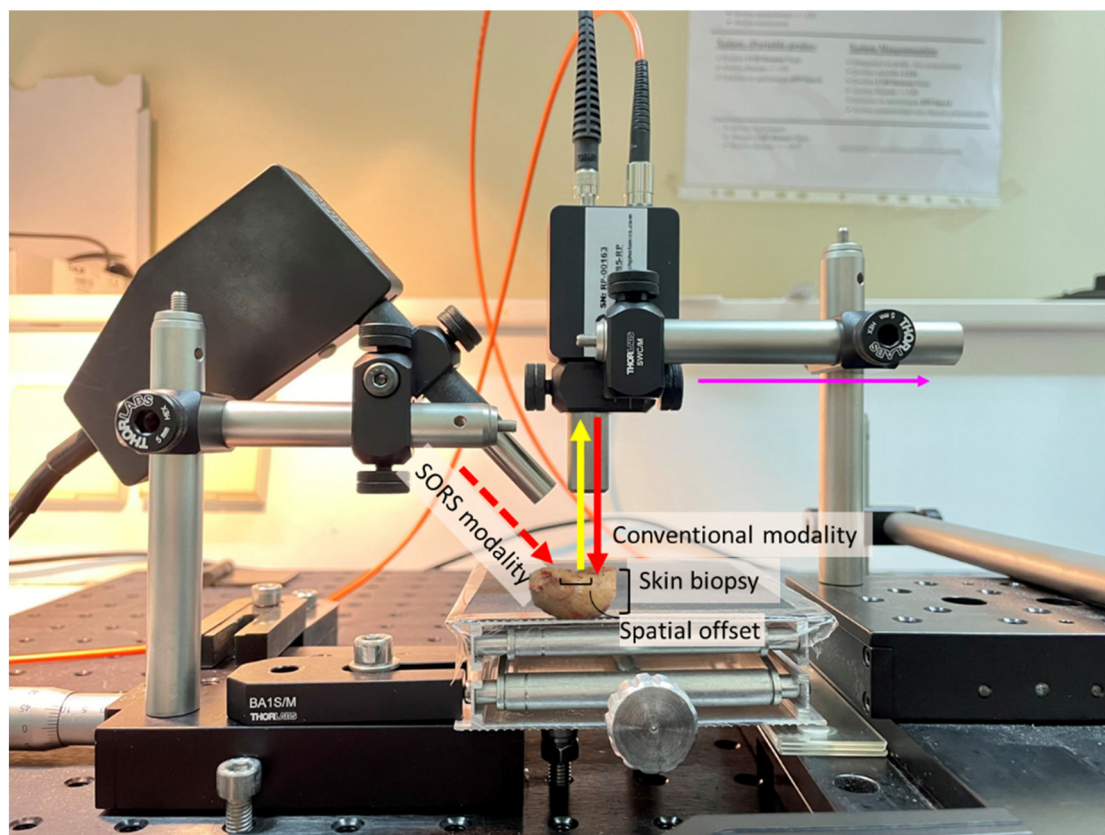


Fig. 2 Raman setup in the conventional (excitation indicated with red solid arrow) and SORS (excitation with red dashed arrow) configurations. The yellow solid arrow indicates the collection probe. A translational XY stage was used to move the collection (magenta arrow) away from the external excitation path and a vertical Z stage to adjust the working distance of the conventional/collection probe.



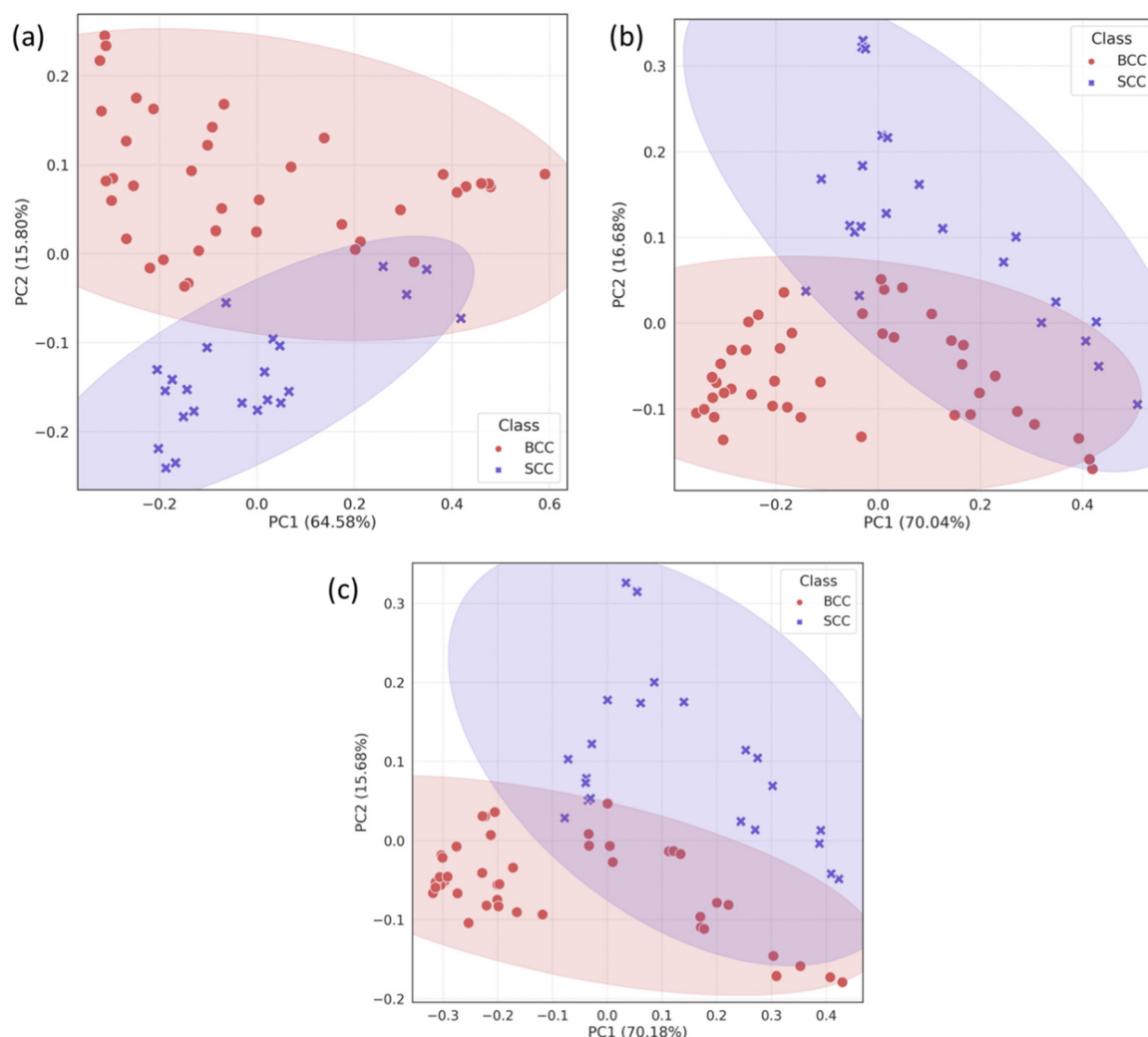


Fig. 3 PCA scatter plots for skin biopsies measured in (a) the conventional back-scattering mode, and (b) zero and (c) 2 mm offset modes. The shaded regions represent the 95% covariance ellipse of each class.

Euclidean distance (0.213 in the conventional *vs.* 0.248 and 0.261 in zero and 2 mm offset, respectively) confirmed this observation. Furthermore, loadings corresponding to PC1 and PC2 are almost identical for the 0 and 2 mm offsets (Fig. 4), implying the same physical basis for the separation in both modes. For both PC1 and PC2 in the 0 and 2 mm modes, the corresponding loadings are positively associated with bands assigned to SCC (Fig. 4). Those bands include 937, 1003, 1125, 1339 and 1640 cm^{-1} and are moving in the opposite direction from 507, 631, 772, 870, 1076, 1189, 1268, 1300, 1435, 1531, 1650 and 1743 cm^{-1} , which are assigned to BCC typical bands negatively associated with the loading for PC2.

To confirm the physical basis of the PCA separation, mean BCC and SCC spectra were subplotted with loadings 1 and 2 for the 0 (Fig. 4a) and 2 mm (Fig. 4b) offsets. As shown in the PCA scatter plots, certain spectral features separating the two subtypes include bands assigned to phenylalanine (1003 and 1339 cm^{-1}), skeletal (937 cm^{-1}) and amide I (1640 cm^{-1}) col-

lagen vibrations, which are more prominent in the SCC type. Spectral bands moving the opposite way (negative) in PC2 loading (Fig. 4) are assigned to tryptophan (772 cm^{-1}), lipids (1076 cm^{-1} , 1300 cm^{-1} and 1650 cm^{-1}) and proteins (amide III at 1268 cm^{-1} and hydroxyproline at 870 cm^{-1}) and are prominent in the BCC group, as previously reported in the literature.^{26,35,36}

Specifically for the spectral bands at 1339 cm^{-1} and 1076 cm^{-1} , they have been previously assigned to nucleic acids, bases (adenine) and backbone as well as lipids and proteins.^{12,35} However, as the strongest nucleic acid contribution (785 cm^{-1}) is not discernible in our data and other bands assigned to nucleic acids (*i.e.* 1531 cm^{-1}) are relatively stable in the processed spectra, we assume that 1076 cm^{-1} is assigned to lipids ($\nu(\text{C}-\text{C})$, $\nu(\text{C}-\text{O})$) and 1339 cm^{-1} to either lipids or phenylalanine. The latter is in line with the trend of the characteristic phenyl ring band at 1003 cm^{-1} , which is also more prominent in the SCC spectra as confirmed by Silveira





Fig. 4 PC1 and 2 loadings of biopsy samples measured with (a) zero and (b) 2 mm SORS, subplotted with the mean Raman spectra of BCC and SCC tissues measured at each mode.

et al. previously.³⁴ This band can be attributed to phenylalanine, but also to keratin as the phenyl ring structure is abundant in the keratin molecule.³⁷ Furthermore, SCC has been shown to positively correlate with phenyl ring content due to the presence of hyperkeratosis,³⁸ which is in agreement with our findings.

We also noticed a stronger contribution of the 1743 cm^{-1} band in the BCC spectra. Although this may be due to lipid contribution from the C=O stretching mode of the ester groups in the glycerol heads of TAG in the adipose tissue underneath the dermis,^{24,39} it may also imply an increased amount of melanin due to more pigmented skin in the BCC patient group.³⁶

By further studying the lipid contributions in PC2 loadings (Fig. 4), we noticed that spectral features of lipids are included in both the BCC and SCC groups. More specifically, PC2 loadings present negative peaks (characteristic of the BCC group) at 1080 cm^{-1} , $1260\text{--}1310\text{ cm}^{-1}$ and 1659 cm^{-1} assigned to unsaturated lipids and mainly triolein from adipocytes, as well as positive peaks (characteristic of the SCC group) at 1128 cm^{-1} and 1283 cm^{-1} assigned to saturated fatty acids of ceramides from the epidermis and phospholipids sphingomyelin and phosphatidylcholine from the cell membrane.³⁴ Estimation of the ratio of characteristic bands from unsaturated (1080 cm^{-1}) and saturated (1128 cm^{-1}) lipids revealed statistically significant differences between the 2 pathology groups in all measurement modes (Fig. 5a).

A negative correlation between BCC and ceramide has already been reported by Tunnell *et al.*³⁸ A comparison of the two groups has demonstrated a higher abundance of ceramide in SCC tissue and lower in triolein, although the results were not as statistically strong.

In terms of collagen content, PCA (Fig. 4) indicates an increased contribution of bands at 937 cm^{-1} and 1640 cm^{-1} , which are assigned to the proline and hydroxyproline backbone and the amide I vibrations of collagen, respectively,⁴⁰ in the SCC spectra compared with the BCC spectra. The difference is shown to be statistically significant when collagen (1640 cm^{-1}) is normalized to protein content (1339 cm^{-1}) (Fig. 5b). Although the abundance of collagen in non-melanoma cancers is not well-studied yet, the negative correlation of collagen with BCC has been confirmed by a small number of studies supporting the low abundance of connective tissue and therefore collagen in BCC sites.^{41,42}

Multivariate factor analysis (MFA)

In order to correlate spectral results with age and sex sample parameters, we employed MFA to assess each mode separately. MFA is an extension of PCA and is able to analyse quantitative (Raman data) and qualitative variables (sex, age, and cancer type) on the same patients by projecting them into a high-dimensional space (Fig. 6).



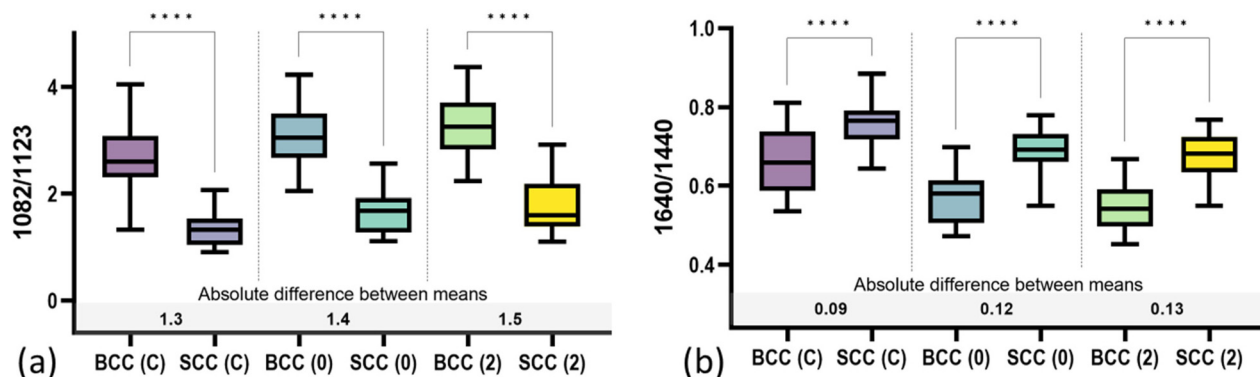


Fig. 5 Mean values of (a) 1082/1123 cm⁻¹ and (b) 1640/1440 cm⁻¹ spectral ratios of band intensities in the different pathology groups and modalities (C: conventional back-scattering, 0: zero offset and 2: 2 mm offset). Asterisks indicate the statistical significance of difference ($p \leq 0.0001$) as determined by the Brown–Forsythe ANOVA ($\alpha = 0.05$), followed by Dunnett's T3 multiple comparisons test.

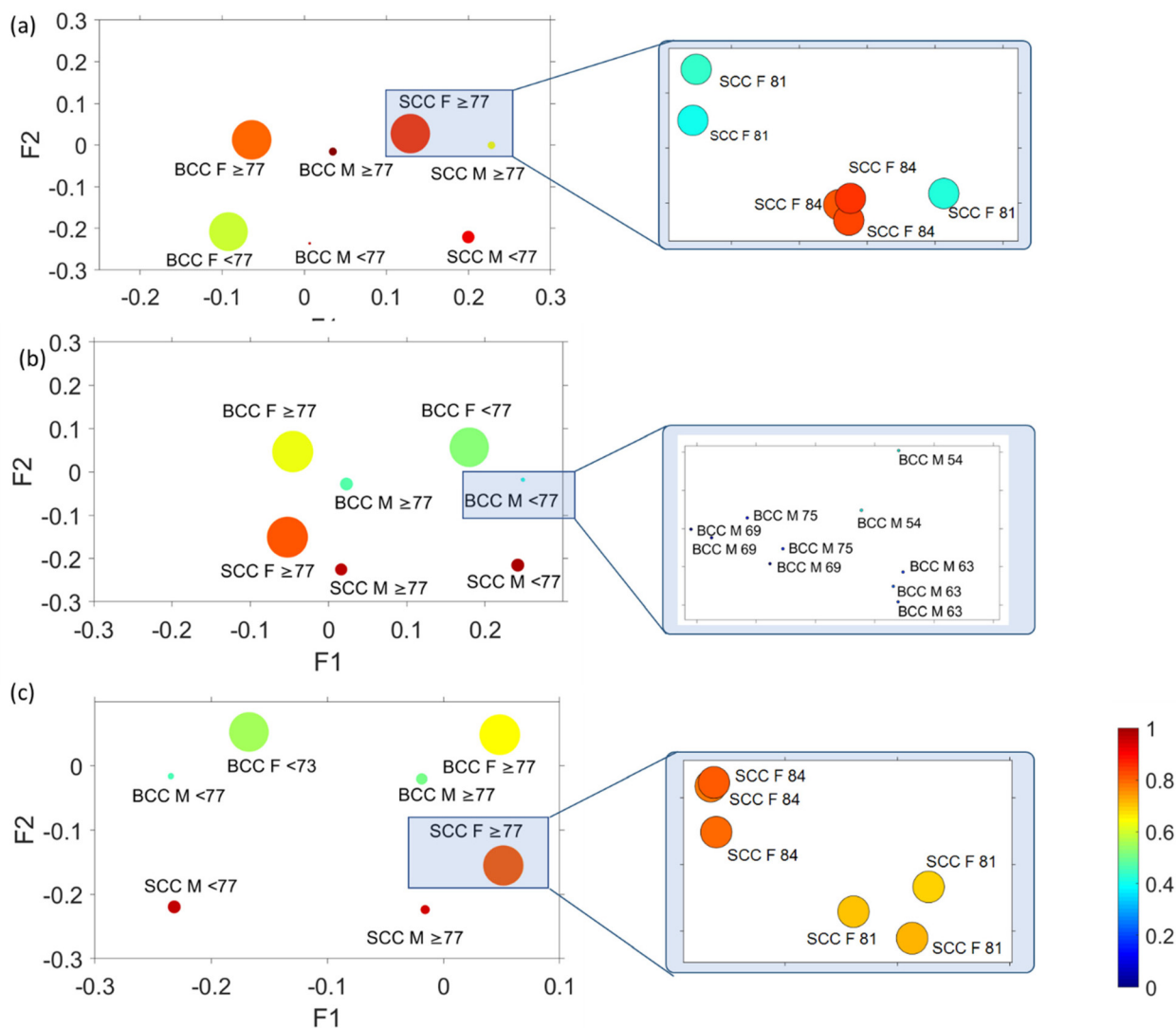


Fig. 6 MFA scatter plots (factor 1 vs. factor 2 vs. factor 3 vs. factor 4) for skin biopsies measured in (a) the conventional back-scattering mode, and (b) zero and (c) 2 mm offset modes. The size of the circles represents factor 3 and circle colour factor 4. Variance explained: conventional back-scattering mode F1 58.78% and F2 20.21%, zero F1 57.30% and F2 19.96% and 2 mm F1 58.93% and F2 19.20%.





Fig. 7 Factor score 2 spectra obtained from MFA plotted against wavenumber in the case of (a) zero and (b) 2 mm offset modes.

In Fig. 6, factor loadings are plotted together for each of the modes, where the size of the circles represents factor 3 and circle colour factor 4. MFA and plotting of factor loading values provide an assessment of the spectral variability between the different pathologies of all patients. In all cases (conventional, 0 mm and 2 mm), we noticed a very strong clustering of variables according to sex (female or male) and age (older or younger than 77 years old). The factor loading values for each distinct group are so similar that an extreme magnifi-

cation is required to observe the individual variables as they highly overlap. Comparing the data with the corresponding histopathological imaging, we noticed that there is no clustering due to the pathology observed in the MFA scatter plot of the conventional mode (Fig. 6a). In contrast, the variables in the conventional mode seem to rather separate along factor loading 2 according to age. In spatial offset modes (Fig. 6b and c), apart from the extremely tight age and sex clustering, the MFA scatter plots also exhibit loose variable separation



Fig. 8 Average factor loadings (normalised and scaled) from MFA. Error bars indicate the standard deviation of the mean.



along factor 2 loading based on tissue pathology (BCC or SCC). As no separation occurs across factor 3 and factor 4, their scores are not analysed further.

Focusing on the two spatial offset cases (Fig. 6b and c), where clustering of different pathology-groups is observed, we noticed that data separation occurred across factor 2. Factor 2 loadings are plotted in Fig. 7, indicating that the main discriminating features in both cases are 875, 1076, 1268, 1300, 1435, 1745, 2850 and 2892 cm^{-1} bands, which correlate positively with the BCC subtype and 937, 1003, 1339, 1640, 1671 and 2948 cm^{-1} bands (characteristic of SCC).

We noticed that the spectral bands in the fingerprint region in factor loading 2, which are responsible for the separation in MFA analysis, are identical to those of PC2 loading, causing BCC–SCC separation in PCA (Fig. 3 and 4). In terms of the high wavenumber region, MFA indicated contributions of lipids and proteins in both pathology groups, which in turn implies the involvement of lipids and proteins in the pathogenesis of both BCC and SCC.

In order to explore the contribution of each factor loading to different measurement modalities, we calculated the averaged factor loading values for all patients (Fig. 8). The factor loading values indicate the strength of the relationship (Pearson correlation) between each modality and the respective factor. Although the factor loadings between different modalities are not directly comparable due to different sampling volumes and measurements, we observe that factor loading 1 (Fig. S2†) is the one that correlates the most with all modalities (although as noted earlier is not responsible for the separation) and decreases slightly with depth. Factor loading 2 (plotted in Fig. 7), which is responsible for pathology discrimination, increases in the 2 mm mode compared to the zero mode.

Conclusions

In this study, we explored the application of SORS technology in non-melanoma cancer diagnosis (BCC and SCC). Our findings highlight spectral separation based on collagen, phenyl ring and lipid vibrations between non-melanoma subtypes. More specifically, we show that bands assigned to protein content (phenylalanine and proline/hydroxyproline in collagen) are more abundant in the SCC type, whereas lipid vibrations are more abundant in the BCC type. A statistically significant difference in unsaturated (triolein) vs. saturated (ceramide) lipid spectral ratio has also been observed in our measurements. The results are in agreement with those of previous studies³⁸ whereas the lack of ceramide in the skin is thought to result in the mutation of basal cells in the epidermis and initiation of BCC growth.⁴³ It should be noted that components such as lipids and water vary significantly between individuals, as well as between anatomical sites of the same individual, and could therefore influence our conclusions.

While the utilization of the confocal modality results in a more precise sampling volume and, subsequently, a better discrimination, we propose that a larger (*i.e.*, deeper) measuring volume could potentially mitigate interpatient variability by increased Raman sampling of skin layers. Additionally, this approach could enable the acquisition of biochemical information from deeper skin layers. Similar studies have utilized a defocused beam to look into a 100 μm depth of skin malignancies, demonstrating that classification accuracy decreases with depth,²⁵ and have eventually chosen an extremely shallow depth measurement in subsequent studies.²⁶

Here, by employing multivariate factor analysis, we conclude that despite a strong impact of patient sex and age, differences in biochemical compositions between BCC and SCC as they are reflected on Raman spectra are significant enough to lead to a pathology-based separation. Our preliminary data demonstrate that Raman spectroscopy in a defocused mode (either 0 or 2 mm) is able to overcome the interpatient variability and therefore constitutes a promising approach for non-melanoma screenings in clinics. We believe that the results of our study will put forward the SORS approach, which will pave the way for an automated and non-invasive skin cancer clinical screening prior to histopathological imaging.

Conflicts of interest

There are no conflicts to declare.

Acknowledgements

This research is co-financed by Greece and the European Union (European Social Fund-ESF) through the Operational Programme “Human Resources Development, Education and Lifelong Learning” in the context of the projects: “Strengthening Human Resources Research Potential *via* Doctorate Research” (MIS-5000432) and “Reinforcement of Postdoctoral Researchers-2nd Cycle” (MIS-5033021), both implemented by the State Scholarships Foundation (IKY).

References

- 1 A. Lomas, J. Leonardi-Bee and F. Bath-Hextall, *Br. J. Dermatol.*, 2012, **166**, 1069–1080.
- 2 M. Ciazynska, G. Kaminska-Winciorek, D. Lange, B. Lewandowski, A. Reich, M. Slawinska, M. Pabianek, K. Szczepaniak, A. Hankiewicz, M. Ulanska, J. Morawiec, M. Blasinska-Morawiec, Z. Morawiec, J. Piekarski, D. Nejc, R. Brodowski, A. Zaryczanska, M. Sobjanek, R. J. Nowicki, W. Owczarek, M. Slowinska, K. Wrobel, A. Bieniek, A. Wozniacka, M. Skibinska, J. Narbutt, W. Niemczyk, K. Ciazynski and A. Lesiak, *Sci. Rep.*, 2021, **11**, 4337.
- 3 K. Seretis, V. Thomaidis, A. Karpouzis, D. Tamiolakis and I. Tsamis, *Dermatol. Surg.*, 2010, **36**, 15–22.



